Journal of Materials Chemistry B

Accepted Manuscript

ROYAL SOCIETY OF CHEMISTRY

www.rsc.org/materialsB

A pH-responsive Amphiphilic Chitosan-Pyranine Core-Shell Nanoparticle for Control Drug Delivery, Imaging and Intracellular pH Measurement

Hao-Syun Chou[1], Meng-Hsuan Hsiao[1], Wei-Yang Hung[1], Tin-Yo Yen[2], Hui-Yi Lin[3*], Dean-Mo Liu[1*]

[1]*Department of Materials Science and Engineering, National Chiao Tung University, 1001 Ta-hsueh Rd. Hsinchu, Taiwan*

[2]*Joint Honours of Biotechnology, Department of Microbiology and Immunology, University of British Columbia / British Columbia Institute of Technology, Vancouver, Canada V6T 1Z4*

[3] School of Pharmacy, China Medical University, TaiChung, Taiwan

*corresponding authors: deanmo.liu@gmail.com and hylin@mail.cmu.edu.tw

Keywords: carboxymethyl-hexanoyl chitosan, pyranine, intracellular pH, core-shell nanoparticle, drug delivery, imaging, camptothecin.

Abstract

A pH-responsive multifunctional core-shell nanoparticle, named CHC-PY nanoparticle, was successfully synthesized through electrostatic interaction of a thin shell of fluorscent pyranine dye (PY) onto amphiphilic carboxymethyl-hexanoyl chitosan (CHC) nanoparticles. Upon encapsulating an anti-cancer drug, camptothecin (CPT), the CHC-PY nanoparticles exhibited an excellent drug loading efficiency (>95%). The resulting CPT-loaded CHC-PY nanoparticles also exhibited efficient cell internalization and high pH-responsive behavior. After being internalized (via efficient endocytosis pathway), the presence of fluorescent PY shell showed a pH-dependent emission characteristic which allowed the internalized CHC-PY nanoparticle acting as an indicator to distinguish the acidic microenvironment of cancerous cells, compared with normal cells. The pH-sensitive PY shell also acted as a modulator to control the CPT release wherein a higher release rate was detected at lower pH value, which is essentially a potential therapeutic niche for anti-cancer purpose. This new type of CHC-PY core-shell nanoparticle provides multiple functionality where a synergistic performance of nanotherapeutics, imaging and even diagnosis at a cellular resolution can be achieved simultaneously.

1. Introduction

One of the most challenging hurdles in the field of biological studies is the construction of the full picture for cancer progression and development. While most of the researches have been focusing on the investigation of enzymatic or genetic causes of cancer formation, very few have investigated in the development of biomedical devices for detection and differentiation of cancer cells from normal cells. Among those who dedicate to the cause, intracellular pH is one of those most intriguing factors in initiating the cascade of cellular and physiological events, including apoptosis,[1] multi-drug resistance (MDR),[2] ion transport,[3] endocytosis,[4] and normal muscle contractions.[5] Abnormality in intracellular pH value is indicative for anomalous cellular function and growth, which often correlates to cancer cell development.[5-8]

Conventional methods of intracellular pH (pHi) measurement include microelectrodes,[9-11] NMR,[12, 13] absorbance spectroscopy and fluorescence spectroscopy.[14-16] These methods have the advantages of spatial and temporal observations for pHi changes, high sensitivity, simple operation processes, and non-destructive to cells. 8-Hydroxypyrene-1, 3, 6-trisulfonic acid, also known as pyranine, has been used as staining agent or pH indicator for cells or tissues.[17, 18] The molecule is an exceptional pH indicator in several aspects： water-soluble, superior chemical and physical stability[19], high cellular retention, high pH-sensitivity, pH-independence for ratiometric measurement, and easy imaging for both *in vivo* and *in vitro*

studies. Nevertheless, when compared to other pH indicating molecules such as BCECF, BCPCF, and 1,4-DHPN,[20-22] pyranine exhibits poor cellular internalization, for intracellular. Most often the internalization of the PY or other pH indicators is achieved through invasive methodologies, such as microinjection, electroporation, and scrape-loading[23]. While effective, these methods cause cell damages that may contribute to the inaccuracy in pH determination. Thus, alternative cellular internalization methods with less detrimental outcomes, such as endocytosis, are required for more efficient and precise measurement of cellular pH and other therapeutic modalities.

Over the past few decades, developments of multifunctional nanocarriers with combined functionalities, such as cell-specific delivery, intracellular imaging, and hyperthermia therapy, have gradually matured in biomedical engineering.[24-27] Several *in-vivo* evaluations have investigated in the effectiveness of several multifunctional nanostructures proposed in the past, and demonstrated correlations between multifunctional nanostructures and improved therapeutic performances.[24, 28] However, it has been relatively rare and challenging to synergize nanocarriers that enables both monitor of intracellular pH and triggered drug release upon a change of physiological pH within normal cells, tumors, or diseased tissues. Therefore, it is important and of our great interest to develop novel nanoparticles that are capable of delivering various therapeutic modalities, while providing stability and functionality for pH measurement under specific microenvironment (e.g., acidic within cancerous cells) upon rapid

cellular internalization.

Here, we report a pH-responsive multifunctional drug delivery nanosystem, which was successfully synthesized through a facile interaction of pyranine (PY), forming shell phase over an amphiphilic chitosan, carboxymethyl-hexanoyl chitosan (CHC), as core phase. This new type of core-shell nanoparticles, termed CHC-PY, demonstrated excellent cytocompatibility, pH- responsive drug release behavior, and intracellular internalization efficiency for both cancerous and normal cells.[29-32] The electrostatic force between the negatively-charged pyranine shell and positively-charged CHC core allowed the core-shell nanostructure to be built efficiently while the outer shell of pyranine is tunable in thickness to modulate drug release profile and emission intensity upon external excitation (scheme 1). This work disclosed a successful design of such a core-shell nanoparticle capable of delivering anti-cancer drug in a pH-sensitive manner and in the meantime, allowing in-situ detection of intracellular pH of various cell lines upon efficient cellular internalization. Besides, the fluorescent emission intensity of the PY illustrated a pH-dependent fashion which enables the resulting core-shell CHC-PY nanosystem acting as an imaging and potential diagnosis agent used to differentiate normal cells and cancer cells through their distinct intracellular physiological pH condition, which renders this new type of CHC-PY nanoparticle a potential multifunctional platform for biomedical uses.

2. Materials and Methods

2.1. Materials

The synthesis of amphiphilic carboxymethyl-hexanoyl chitosan (CHC) was reported previously and has been described in detail in a number of publications from our lab.[29, 30] The hydrophobic hexanoyl group and hydrophilic carboxymethyl group allowed the CHC molecules to self-assemble in neutral aqueous medium into nanoparticles of 100-200 nm in diameter, giving rise to a positively-charged colloidal-geometry in the resulting CHC nanoparticles. Pyranine was bought from Tokyo Chemical Industry and was used as received without further purification. The anti-cancer drug, (S)-(+)-Camptothecin (CPT) (Mn = 348.36, Approx. 95%HPLC), was purchased from Sigma-Aldrich and used as received.

2.2. Preparation of CHC-PY nanoparticles

10mg CHC powder was first dispersed in 5 mL distilled water. The solution was gently shaken at room temperature for 24 hrs, and then sonicated using Automatic Ultrasonic Processor, UH-500A (China) at 35W for 30 sec. Pulse function with 5.0 sec intervals and 1.0 sec intervening pulse-off period was used during sonication to prevent building-up of excessive heat. The sonication process was repeated three times until an optically clear solution was obtained. According to previous studies, the amphiphilic CHC macromolecules self-assemble into spherical nanoparticles with an average size of 100-150 nm in diameter

after dispersing in aqueous solution. The stabilized colloidal CHC nanoparticles possess a positive surface charge of 34.3 ± 0.7 mV, which allow for deposition of the negatively charged PY molecules (-6.6 ± 1.3 mV) to form a corona phase surrounding the CHC core via strong electrostatic interaction.

Five mL pyranine solutions at concentrations ranging from 0.1 mg/ml to 0.3 mg/ml were prepared and added in a drop-wise fashion into aliquots of CHC colloidal samples with a fixed concentration of 1mg/ml. The mixtures were stirred at room temperature for 1hr, and then centrifuged at 12,000 rpm for 10 min under 20°C, from which the precipitates were decanted to obtain CHC-PY nanoparticles. Amount of pyranine adsorbed onto the CHC-PY nanoparticles was analyzed by measuring the UV absorbance of the supernatant that contained free pyranine, which the measured value was then used to calculate the amount adsorbed onto the CHC nanoparticles. The wavelength of pyranine in UV spectrum is at 460 nm, and the supernatant was dilute in pH 7 PBS buffer to control the pH value of solution.

2.3. Preparation of drug loading nanoparticles

Drug entrapment into CHC-PY nanoparticles was carried out by the following procedures. Dimethyl sulfoxide (DMSO, reagent grade, Sigma Inc.) was used as a co-solvent to dissolve the hydrophobic drug CPT, and the solution was diluted with D.I. water (0.5/9.5 v/v) to reach a working concentration of 100 μg/ml. Following, powdered form of CHC was added to the

solution until a final concentration of 2 mg/ml CHC was achieved. The mixture was stirred at ambient temperature for 24hr for formation of CHC nanoparticles and efficient drug encapsulation. After preparation of CPT-loaded nanoparticles, pyranine solutions of different concentrations were added to aliquots of CPT-loaded nanoparticle suspensions, and stirred at room temperature for 1hr. The solutions were then centrifuged under 20℃ at 2000 rpm for 5 min, followed by another cycle at 12000 rpm for 10 min to obtain a final CPT-loaded CHC-PY nanoparticles.

Concentration of free CPT (not being encapsulated) in the supernatant of each solution was measured in triplicate using High Performance Liquid Chromatography (HPLC, Aglient Technologies 1200 Series) at wavelength of 367 nm, a characteristic absorption band of CPT. The measurement was carried out using a 150mm×4.6mm C18 column of 5μm in length, with a constant flow rate of 0.8 mL/min. The mobile phase was composed of a D.I. water aqueous phase (A) and an acetonitrile organic phase (B), in a volume ratio of A : B = 3 : 2 (v/v). Drug encapsulation efficiency (EE) can be calculated following the equation below:

$$\mathrm{EE} = \frac{(A-B)}{A} \times 100\% \quad (1)$$

Where A is the total amount of the CPT, B is the amount of CPT remaining in the supernatant.

2.4. Characterization of CHC-PY nanoparticles.

The surface charge of CHC-PY nanoparticles was characterized via zeta potential (Delsa Nano C, Beckman Coulter, U.S.) at pH 6. Particle size was measured using dynamic light scattering spectroscopy (DLS, BI-200SM Goniometer DLS, Brookhaven Inc., Holtsville, NY), and structural image was acquired using transmission electron microscopy (TEM, JEOL2100, Japan) with voltage of 200keV for optimal imaging quality. TEM samples were prepared by soaking a carbon-coated copper grid in CHC-PY solution and then dried at room temperature.

2.5. CPT Release Behavior

Drug release behavior from the CPT-loaded CHC-PY nanoparticles was determined by measuring the concentration of CPT in 1 mL PBS solution at different release conditions and time durations. After centrifugation at 8,000 rpm, the supernatant that contained the released drugs was subjected to HPLC characterized at wavelength of 367 nm for CPT measurement. Each CPT concentration was obtained in triplicate measurements.

Drug release profiles of the CHC-PY nanoparticles were further analyzed using the power law equation:[33, 34]

$$\frac{M_t}{M_\infty} = Kt^n \quad (2)$$

Where M_t/M_∞ is the percent of the drug release at time t, K is a rate constant incorporating structure and geometric characteristic of the release device, and n is a characteristic exponent

indicative of the release mechanism.

2.6. In vitro cytotoxicity and therapeutic efficacy

Lung adenocarcinoma cells (A-549) was cultured in 96 well culture plate with 1×10^4 cells for 24 hours before treatment. 2 mg/ml CHC-PY0.2 nanoparticles, 2 mg/ml CPT-loaded CHC-PY0.2 nanoparticles, and 192.2 μg/ml free CPT were added, respectively. After incubation for 24 hours, MTT solution (0.5mg/ml) was added and reacted for 4 hours, then, DMSO was added to dissolve the purple formazan and measured by a MicroELISA reader (GDV, DV 990BV4, Italy) at 595 nm. Cell viability was determined by calculation according to the following equation:

Cell viability (%) = $(A_{sample} / A_{control}) \times 100\%$

Where A_{sample} is the absorbance of sample and $A_{control}$ is the absorbance of control.

2.7. Intracellular pH Determination.

Three cell lines of human origins were cultured in order to investigate the intracellular pH value with different oncological statuses: intestinal epithelial cells (IEC-6), representing normal cells, and heterogeneous human epithelial colorectal adenocarcinoma cells (CaCo-2) and lung adenocarcinoma cells (A-549), representing cancer cells. 1×10^6 cells of each aforementioned cell lines were first cultured on a 10cm-cell culture dish. The cultures were

then incubated overnight with an addition of 4 mg/ml CHC-PY nanoparticles solutions. The cells were then harvested and re-suspended in 1 ml of D.I. H_2O, and the suspensions were measured for UV absorbance at characterized wavelengths of 460 and 405nm. Correction for the signal value, Rex, was calculated using the following formula:

$$\text{Rex} = (\lambda\text{exc.}\,460\ \text{nm}/\lambda\text{exc.}\ 405\ \text{nm}) \quad (3)$$

The calculated values of Rex were further converted to Log(Rex) using the following formula:

$$\log(Rex) = 0.398\text{x} - 2.983 \quad (4)$$

Where x is the intracellular pH value (supporting information figure S1). The conversion allowed for the analysis of logarithmic correlations between sample absorbance and both extracellular pH and pHi.

2.8. Intracellular imaging

Both IEC-6 and CaCo-2 cell lines were employed as model cell representing normal and cancer cells, respectively, to evaluate the imaging capability of the CHC-PY nanoparticles. Cells were cultivated on glass coverslips for 24 hrs, and treated with the 0.1% (w/w) CHC-PY nanoparticles for different incubation durations., After washing with phosphate buffer saline (PBS) to remove excess nanoparticles, the cells were mounted on fresh glass slides, and analyzed by Multiphoton and Confocal Microscope System (MCMS) (TCS-SP5-X AOBS,

Leica, Mannheim, Germany) with 470nm laser excitation and 405nm UV light excitation. The ratio of I_{405}/I_{470} was determined by the averaged values (in quadruplicate measurements) of measured emission intensity of Ex 470 and Ex 405, where the difference in the ratio can be easily distinct between normal cells and cancer cells due mainly to the difference in respective intracellular pH value.

3. Results and discussion

3.1. Pyranine shell formation on CHC nanoparticles

Electrostatic attraction between negatively-charged pyranine and positively-charged CHC nanoparticles was responsible for the formation of CHC-PY core-shell nanoparticles. Calculations of pyranine deposition were based on the UV spectrum of the supernatant after centrifugation. The amount of pyranine deposited onto the surface of CHC nanoparticles was dependent on the concentration of pyranine added into the CHC solution; an inclining trend in pyranine deposition with increasing pyranine concentration was observed (Table 1). Such phenomenon was believed to be the result of pyranine deposition equilibrium, which would be driven towards deposition as the concentration of added pyranine increased. This ultimately led to higher coverage of pyranine on the surface of CHC cores, and gave rise to a decreased zeta potential and an increased size of the resulting CHC-PY nanoparticles (Columns 2 and 3 in Table 1).

Table 1. Physical characteristics of CHC-PY nanoparticles and drug encapsulation efficiency with different CHC : PY ratios. The numbers of sample I.D., such as 0.1, 0.15, 0.2, and 0.3, mean the pyranine concentration at the prepared solutions.

Sample I.D.	PY deposition [μg/ml]	Zeta Potential [mV]	Mean size [nm]	Encapsulation efficiency [%]
CHC	0	34.3 ± 0.7	107.7 ± 1.9	90.7
CHC-PY0.1	70.4 ± 3.6	32.1 ± 1.4	113.5 ± 2.9	95.4
CHC-PY0.15	119.9 ± 3.8	25.3 ± 2.3	119.6 ± 1.5	95.8
CHC-PY0.2	162.2 ± 6.2	18.5 ± 2.7	123.7 ± 2.7	96.1
CHC-PY0.3	260.4 ± 7.2	8.7 ± 1.8	132.6 ± 0.5	96.5

3.2.Colloidal Properties of CHC-PY nanoparticles.

The effect of pyranine on zeta potential and mean size of the CHC-PY nanoparticles was investigated using samples prepared with different pyranine concentrations. The zeta potential of resulting CHC-PY nanoparticles, as given in Table 1, became weaker with increasing concentration of pyranine. This observation was a result of charge neutralization between the positively-charged CHC surface and negatively-charged pyranine upon deposition. As aforementioned, when the total contributed charge of pyranine intensifies, the amount of

deposited pyranine on the CHC nanoparticles increase. This leads to two outcomes, both of which contribute to the decline in zeta potential of CHC-PY nanoparticles: (a) the shielding of positive charge of CHC nanoparticle core by the negatively-charged pyranine, and (b) gradual decrease in overall positive charge from 34.3 mV to 8.7 mV as the pyranine concentration increases from 0 to 0.3 mg/ml. This means that the intensity and nature of the CHC-PY nanoparticles are highly tunable, rendering a broad spectrum of colloidal properties of the nanoparticles that can potentially be utilized for a range of biomedical applications.

The sizes of the final CHC-PY nanoparticles determined using the dynamic light scattering spectroscopy (DLS) (Table 1) were 107 nm, 113 nm, 120 nm, 124 nm and 133 nm as the pyranine increased from 0 mg/ml, 0.1 mg/ml, 0.15 mg/ml, 0.2 mg/ml to 0.3 mg/ml, respectively. This corresponded to an average thicknesses of the pyranine shells ranging from 0 nm, 3 nm, 6.5 nm, 8.5 nm to 13 nm, respectively. A linear correlation between shell thickness and pyranine concentration, as shown in Fig.1, was observed and was indicative of a zero-order pyranine deposition kinetic that followed a relatively constant electrostatic-dominating mechanism. Since the molecular size of pyranine is approximately 1.5 nm and exhibits a bulky shape, it was then estimated that the formed shell could be 2, 4, 6, and 9 layers of deposited pyranine by the assumption of a uniform deposition throughout the shell forming process. Since the CHC core is near spherical in shape as shown in Fig.2(a), TEM examination was used to confirm the presence of a core and outer shell layer in the

CHC-PY0.2 nanoparticles sample, as shown in Fig.2(b). The image indicated the pyranine successfully deposited on the surface of the CHC core in a random fashion, with patches of the shell being slightly thicker than the rest of the nanoparticle surface. While the underlying reason for the unevenness of pyranine deposition along the core surface is unclear, we postulated that the strong positive charge exhibited by the non-coated CHC core favours a fast non-homogeneous pyranine distribution at the beginning of coating process. As more pyranine is brought to the quick-forming CHC-PY nanoparticles, the electrostatic attraction exerted by the CHC-PY surface becomes weaker, thus resulting in a more gradual deposition of pyranine until the deposition equilibrium is reached.

3.3. Structural stability of pyranine shell

Once the pyranine molecules were successfully deposited onto the CHC core, it became critical to investigate the stability of the deposited pyranine, since the electrostatic attraction force provided the necessary energy for the non-covalent bonds between the CHC and pyranine molecules. The bonds may suffer from breakage in the form of pyranine desorption in diluted environments (i.e. the circulatory system) or long-term shelf storage. This may further lead to a change in properties such as spectral emission intensity, drug release profile due to decreasing surface coverage, surface net charge and more, which ultimately weaken the desired performance of the encapsulated drugs. Therefore, characterization of the pyranine

shell stability is absolutely essential to ensure the practical niche of the resulting core-shell nanoparticle. The amount of pyranine adhered to the surface of the CHC nanoparticle under different pH environments was evaluated by UV spectrum. Diluted media of different pH values, as well as different collection time periods of 0, 0.5, 24, and 120 hr, were selected to carry out the investigation.

The third column of Table 2 provides the remaining amount of pyranine staying on CHC core that was detected at first 30 min upon dilution test, with a starting pyranine concentration normalized as 100% (t=0, second column). 2% of remaining pyranine (from 100% reduced to 98%) was measured at pH 4, wherein 7% (100% → 93%) at pH 5, 14% (100% → 86%) at pH 6, and 21% (100% →79%) at pH 7 were measured. Such trend clearly revealed a result of pyranine desorption from the CHC-PY nanoparticles. However, the desorption rate declined significantly over a subsequent duration of nearly 120 hr across all pH values, with only 5% (98% → 93%) at pH 4, 5% (93% → 88%) at pH 5, 6% (86% →80%) at pH 6, and 8% (79% →71%) at pH 7. This implied that the remaining pyranine molecules were structurally stabilized on the CHC core surface. This suggests that the initial pyranine desorption during the first 30 minutes is fast and dependent on the environmental pH. The surface charge of CHC core becomes weaker as the solution pH increases with larger dilutions (IEP is closed to pH7.5 for CHC core nanoparticle, see Figure S2), which in turn reduces the electrostatic interaction between the CHC core and pyranine until sufficient amount of pyranine has been

diluted. This loss of electrostatic attraction force causes the adhered pyranine to fall off the CHC-PY nanoparticles, leading to the reduction of outer shell thickness, as well as the positive addition of the overall surface charge. As the surface charge of CHC-PY nanoparticles increases with reducing outer shell thickness, the shielding effect brought by the outer shell weakens and allows for even higher stability for the electrostatic attractive force between the remaining adhered pyranine and the CHC core. Thus, the stabilization between pyranine outer shell and CHC core is achieved through the increase of electrostatic attraction force; the pyranine molecules found on the utmost region of the shell are subjected to a reduced force of electrostatic attraction, making them less likely to stay adhered upon a change toward more basic pH.

In comparison to the initial pyranine desorption stage, further desorption of the adhered pyranine during the subsequent 120-hrs observation period was more gradual and less pronounced. This was especially prevalent at higher pH values, which indicated that the pyranine molecules adhered firmly on the core surface. This observation confirmed the use of pyranine to create a stable shell structure with great potential for biomedical applications.

Table 2. Remaining amount (normalized) of pyranine staying on the nanoparticle under different pH values for various time intervals (t) of incubation.

pH value	t=0 [%]	t= 0.5hr [%]	t=24hr [%]	t=120hr [%]
pH 4	100	97.62	95.24	92.86
pH 5	100	92.77	90.36	87.95
pH 6	100	86.08	82.28	79.75
pH7	100	78.75	75.00	71.25

3.4. Anticancer drug encapsulation

Once the stability of the pyranine shell was experimentally confirmed, the applicability of the resulting CHC-PY nanoparticles for drug delivery was evaluated using a highly hydrophobic drug, CPT, as the model molecule. The encapsulation efficiency of CPT was optimized at >95% for all CHC-PY compositions prepared in this work as given in Table 1. It is relatively interesting to learn, in comparison with pure CHC core, that higher drug loading efficiency was achieved with increasing pyranine deposition. One plausible reason was the fast surface coverage by pyranine upon mixing the CPT-containing CHC core and pyranine, wherein a shell was readily built up with increasing thickness as pyranine increased, to form an effective barrier to inhibit the early-phase release of the CPT (see forthcoming section), resulting in a higher drug payload. This finding indeed gives a synergistic benefit toward the

multifunctional drug delivery system currently prepared, where higher drug payload and effective barrier for controlled drug delivery can be achieved synergistically.

3.5. Drug release behavior

3.5.1. Effect of pyranine concentration

Figure 3a shows the resulting drug release profiles for the CPT-loaded CHC-PY nanoparticles prepared with various pyranine concentrations, from 0.1 mg/ml to 0.3 mg/ml, in PBS buffer of pH=7. As expected, the release profile was significantly slower at higher pyranine concentrations, confirmed the formation of thicker pyranine shell that can efficiently effectively reduce the burst-like release of the CPT, instead, a slow and sustained release profile was achieved.

A closer examination on the release profiles of drug-loaded CHC-PY nanoparticles with lower pyranine concentrations, i.e., 0.1 mg/ml and 0.15 mg/ml, exhibited similar burst-elution behaviors to that observed in drug-loaded CHC core phase alone. We postulated that this could be due to the early-stage desorption of pyranine at higher solution pH (in the case, pH = 7), leading a rapid thinning of the outer shell that allows CPT to leak through easily and eluted into the diluting medium. However, the early-phase burst-like behavior can be effectively reduced with increasing pyranine of more than 0.2 mg/ml, which is in good agreement with aforementioned analysis on the structural stability of the shell.

On the other hand, the effect of pyranine shells on drug release kinetics can be evaluated from Equation 2, where the reaction order n of CHC-PY nanoparticles was determined experimentally to be ranged from 0.16 to 0.20 (Table 3), suggesting a quasi-Fickian diffusion mechanism for the drug-loaded nanoparticles. The rate constant K laid between the 3.8 (CHC-PY0.3) and 6.0 (CHC-PY0.1), which demonstrated an inverse relationship with respect to increasing shell thickness (Figure 4). The trend further confirmed the inhibitory effect of pyranine outer shell on CPT elution via the increase in diffusion pathway length for the drug molecule to travel through.

Table 3. Kinetic parameters: reaction order (n) and rate constant (K), obtained as a result of model fitting for the CPT release from CHC-PY nanoparticles with various starting pyranine concentrations.

sample	**n**	**K**	**R^2**
CHC	0.29 ± 0.01	5.88 ± 0.19	0.9949
CHC-PY0.1	0.21 ± 0.01	5.97 ± 0.08	0.997
CHC-PY0.15	0.19 ± 0.01	5.51 ± 0.19	0.9755
CHC-PY0.2	0.16 ± 0.02	5.04 ± 0.23	0.9399
CHC-PY0.3	0.18 ± 0.03	3.83 ± 0.28	0.9018

3.5.2. Effect of solution pH

The influence of solution pH on the CPT release profile was examined using CHC-PY0.2 as representative example, since this composition demonstrated high stability of the pyranine shell over a wide range of pH values. Figure 3b shows the CPT release profile at various pH

values, ranging from 4 to 7. The rate of CPT release decreased with increasing solution pH, signifying a rapid release of CPT under acidic condition and an inversely-proportional relationship with solution pH up to a near-physiological pH (pH 7). This pH-responsive behavior can be explained by two earlier observations: (a) at higher pH, the shell thickness reduced as a result of early-stage desorption, i.e., *ca.* 20% pyranine loss at pH=7, which corresponded to *ca.* 8% of shell thickness reduction, and (b) the surface charge of the CHC approached neutral. Both of these factors contributed to a more compacted CHC core structure, resulting in a significant synergistic reduction of the CPT adhesion and coverage.

In contrast to the significant loss of adhered CPT under acidic environment, the reduction in shell at lower pH was relatively less. However, an observable swelling of CHC core was noted, and was postulated as a result of intra- and inter-molecular repulsion due to the protonation the amine groups found in CHC. It appears, as shown in Fig.3b, that the repulsion-induced swelling became more pronounced with decreasing pH, which corresponded to a simultaneous decrease in the drug release. We then conclude that the pH-responsive release behavior of CPT from the CHC-PY nanoparticles is virtually an interplay of pH responsiveness between the pyranine shell and CHC core. The nanoparticles appears to be a highly promising nanoplatform for anti-cancer therapeutics, as a higher drug release rate at acidic environment is more therapeutically favorable since some cancerous cells or tumors have been recognized to be more acidic in its intracellular

microenvironment.[35]

3.6. In vitro cytotoxicity and therapeutic efficacy

The cytotoxicity of CHC-PY nanoparticles and the therapeutic efficacy were evaluated with A549 cells by MTT assay for 24 hours. As shown in Fig 5, cell viability of A549 treated with CHC-PY0.2 nanoparticles still remained above 90 %, which is an evidence that the nanoparticle is with good biocompatibility and low cytotoxicity. The CPT loaded CHC-PY0.2 nanoparticles (CPT-CHC-PY) and free CPT drug showed 70% and 50 % cell viability, respectively. The concentration of free CPT was controlled to the same concentration in CPT-CHC-PY nanoparticle to evaluate the therapeutic efficacy of the nanoparticle. The difference of therapeutic efficacy is due to the slow release property of CPT-CHC-PY nanoparticle. These evidences indicate that the CPT-CHC-PY nanoparticle is good candidate for loading hydrophobic anticancer drug and drug delivery because of its good compatibility and low toxicity.

3.7. Intracellular pH measurement

Intracellular pH is crucial in understanding many biological functions, including cell permeability, enzymatic activity, cell growth, cell differentiation, and cell apoptosis. In order to investigate the potential applicability of CHC-PY nanoparticles towards the measurement

of intracellular pH, as well as to study the intracellular behaviors of the nanoparticles in cancer cells and normal cells, normal cell line (IEC-6) and cancer cell lines (CaCo-2 and A549) were separately incubated with CHC-PY0.2 nanoparticles. Ratiometric probe was used to measure the excitation spectrum at wavelengths of 460 nm and 405 nm, and the ratios, or Rex values, were calculated based on the measured primary maxima of the two wavelengths. As observed in the normalized excitation spectrum of CHC-PY0.2 nanoparticles (Fig. 5a), increase in buffer pH leads to an increase in secondary maximum at 460 nm, which is the excitation wavelength of unprotonated pyranine. Meanwhile, the primary maximum at 405 nm, which is the excitation wavelength for protonated pyranine, remained relatively stable.

Fig 5b shows the excitation spectra for the three cell lines, which are normalized to the maximum 405 nm peak. IEC-6 showed the strongest absorbance at 470 nm comparing with the other two cell lines, followed by CaCo-2 and A-549. This result indicated that the CHC-PY nanoparticles demonstrated an excellent and precise pH-responsive behavior in terms of normal cells and cancer cells via specific sensitizing of the intracellular pH value.

Results of the excitation spectra were then compiled and calculated for both Rex and log (Rex) of CHC-PY0.2 nanoparticles in different cell lines (Table 4). The calculated values of log (Rex) can then be used to approximate the pH value from the calibration graph. Calculated values indicated that the intracellular pH of IEC-6 was approximately 7.02, whereas CaCo-2 and A-549 appeared to be more acidic, with pH values of 6.30 and 6.51,

respectively. The results were in excellent agreement with those proposed by literature reports, and confirmed a highly-pH sensitized technique to monitoring the subtle variation in intracellular pH upon therapeutic treatment[35-38]

Table 4. Calculated pH values for three types of cells line.

Cell line	Calculated pH value after 24 hrs incubation
IEC-6	7.02 ± 0.11
CaCo-2	6.30 ± 0.02
A-549	6.51 ± 0.06

The CHC-PY nanoparticles successfully predicted over a certain accuracy the intracellular pH value of normal cells (IEC-6) and cancer cells (CaCo-2 and A549). The pH-sensitive emitting nature of the fluorescent PY rendered the resulting CHC-PY nanoparticles capable of distinguishing the physiological microenvironment between cells of differing nature, to be specific, normal cells and cancer cells as disclosed in this work, by their specific fluorescent emitting behavior. In Fig.5b, the nanoparticles show a constant absorbance value at 405 nm under different pH levels but the absorbance varied at 470 nm. The intensity of the absorbance at 470 nm increased with the pH value, which can be used as an indicator to distinct cells of various physiological nature via a simple cell culture protocol.

The CHC-PY nanoparticles internalized in IEC-6 and CaCo-2 were excited by λ_{ex} 405 nm and λ_{ex} 470 nm and calculated the ratio of the emission intensity at 510 nm. As illustrated in

Figure 6, the emission intensity with λ_{ex} 405 nm shows similar spectra between IEC-6 and CaCo-2, but a notable difference is clearly detected while emitting with λ_{ex} 470 between IEC-6 and CaCo-2. The emission intensity of the nanoparticles with IEC-6 was nearly 2.5-fold higher than that with CaCo-2, suggesting the capability of the CHC-PY nanoparticles in identifying the physiological difference between normal cells and cancer cells.

However, there had a problem that the CHC-PY nanoparticles were in cytoplasm or organelles after endocytosis. Different location of cells existed different pH values that had great effect on the result of pH measurement, such as lysosome that was at much acidic environment. From Fig.5b, the spectrum showed macroscopic results that revealed what kind of environment the CHC-PY nanoparticles were in. As the macroscopic results, pH 7 for normal cells and pH6.5 for cancer cells conformed to other researches, which confirmed the CHC-PY nanoparticles can measure correct intracellular pH values, and didn't need to care about which location of cells the CHC-PY nanoparticles were in.

3.8. Intracellular Imaging

Besides its pH monitoring capability, in Figure 7, the nanoparticles, after being internalized within the cells, were excited by 405 nm and a clear fluorescent image was visually detected, indicating that the CHC-PY nanoparticles were highly accessible through cell membrane by endocytosis while its fluorescent emitting behavior was kept identical. The fluorescence

intensity of both nanoparticles in IEC-6 cells and CaCo-2 cells were weakened while excited by 470 nm light, as illlustrated in Figure 7c and 7g. However, the fluorescent intensity (brightness) of the nanoparticles in CaCo-2 cells was conspicuously lower than that in IEC-6 cells, which is virtually a result of cell nature, as given in Table 5, the value of I_{405}/I_{470} for IEC-6 (normal) cells and CaCo-2 (cancer) cells is 4.29 and 40.63, respectively. As a result, both the pH-dependent imaging contrast and pH monitoring capabilities ensure this CHC-PY nanoparticles a new multifunctional nanoplatform with enhanced nanomedicinal potential for a number of biomedical uses.

Table 5. The brightness value of different excitation and cells. (n=4)

Cell line	I_{405}	I_{470}	I_{405}/I_{470}
IEC-6	4.91	1.13	4.29 ± 0.50
CaCo-2	3.1	0.08	40.63 ± 2.96

4. Conclusion

A pH-responsive multifunctional drug delivery nanoparticle was successfully synthesized by forming a core-shell nanostructure, composed of a carbomethyl-hexanol chitosan (CHC) core and pyranine dye as a thin shell. The core-shell nanostructure exhibited a stable and tunable colloidal behavior in terms of size, surface charge, and fluorescent emission

characteristics. The CHC-PY nanoparticles exhibited a strong synergizing performance with high drug encapsulation efficiency (>95%), efficient cellular internalization, pH-responsive drug release behavior, cell imaging capability, as well as intracellular pH measurement. The pH-sensitizing property renders the CHC-PY nanoparticles a powerful indicator to distinguish physiological pH nature between normal cells and cancer cells via fluorescent spectrum and imaging modality. Such a new multifunctional nanoplatform allows nanotherapeutic strategy to be tunable according to practical needs ranging from therapeutics, imaging to diagnosis or a combination therapy. Further investigation of the core-shell CHC-PY nanoplatform toward animal model is under development which is intended to find niche performance toward better clinical translation.

AUTHOR INFORMATION

Corresponding Author

* E-mail: deanmo_liu@yahoo.ca. Tel +886-3-5712121(ext. 55391);

Acknowledgements

This work was financially supported by the National Science Council of the Republic of China, Taiwan, and the instrument of Multiphoton and Confocal Microscope System (MCMS) and DLS is supported by College of Biological Science and Technology,

National Chiao Tung University, Taiwan, R.O.C.

Reference

1. D. Pérez-Sala, D. Collado-Escobar and F. Mollinedo, *Journal of Biological Chemistry*, 1995, 270, 6235-6242.
2. S. M. Simon and M. Schindler, *Proceedings of the National Academy of Sciences*, 1994, 91, 3497-3504.
3. A. Varadi and G. A. Rutter, *Endocrinology*, 2004, 145, 4540-4549.
4. R. A. Gottlieb, J. Nordberg, E. Skowronski and B. M. Babior, *Proceedings of the National Academy of Sciences*, 1996, 93, 654-658.
5. A. J. Bullock, R. A. Duquette, N. Buttell and S. Wray, *Pflügers Archiv European Journal of Physiology*, 1998, 435, 575-577.
6. H. Izumi, T. Torigoe, H. Ishiguchi, H. Uramoto, Y. Yoshida, M. Tanabe, T. Ise, T. Murakami, T. Yoshida, M. Nomoto and K. Kohno, *Cancer Treatment Reviews*, 2003, 29, 541-549.
7. T. A. Davies, R. E. Fine, R. J. Johnson, C. A. Levesque, W. H. Rathbun, K. F. Seetoo, S. J. Smith, G. Strohmeier, L. Volicer, L. Delva and E. R. Simons, *Biochemical and Biophysical Research Communications*, 1993, 194, 537-543.
8. J. Zhang, L. Wu, F. Meng, Z. Wang, C. Deng, H. Liu and Z. Zhong, *Langmuir*, 2011, 28, 2056-2065.
9. A. Kotyk and J. Slavík, *Intracellular pH and its Measurement*, CRC, 1989.
10. J. A. Thomas, R. N. Buchsbaum, A. Zimniak and E. Racker, *Biochemistry*, 1979, 18, 2210-2218.
11. A. De Hemptinne, *The Journal of physiology*, 1979, 295, 5P.
12. V. V. Kupriyanov, B. Xiang, J. Sun, O. Jilkina and R. Deslauriers, *Biochimica et Biophysica Acta (BBA) - Molecular Basis of Disease*, 2002, 1586, 57-70.
13. M. Vermathen, M. Marzorati, P. Vermathen and P. Bigler, *Langmuir*, 2010, 26, 11085-11094.
14. G. Bright, G. Fisher, J. Rogowska and D. Taylor, *Methods Cell Biol*, 1989, 30, 157-192.
15. J. Han and K. Burgess, *Chem. Rev*, 2010, 110, 2709-2728.
16. S. Ogikubo, T. Nakabayashi, T. Adachi, M. S. Islam, T. Yoshizawa, M. Kinjo and N. Ohta, *The Journal of Physical Chemistry B*, 2011, 115, 10385-10390.
17. K. A. Giuliano and R. J. Gillies, *Analytical biochemistry*, 1987, 167, 362-371.
18. C. C. Overly, K. D. Lee, E. Berthiaume and P. J. Hollenbeck, *Proceedings of the*

National Academy of Sciences, 1995, 92, 3156-3160.
19. N. Barrash-Shiftan, B. Brauer and E. Pines, *Journal of Physical Organic Chemistry*, 1998, 11, 743-750.
20. T. Rink, R. Tsien and T. Pozzan, *The Journal of cell biology*, 1982, 95, 189-196.
21. T. Speake and A. C. Elliott, *The Journal of physiology*, 1998, 506, 415-430.
22. I. Kurtz and R. S. Balaban, *Biophysical journal*, 1985, 48, 499.
23. B. S. Gan, E. Krump, L. D. Shrode and S. Grinstein, *American Journal of Physiology - Cell Physiology*, 1998, 275, C1158-C1166.
24. S. Sengupta, D. Eavarone, I. Capila, G. Zhao, N. Watson, T. Kiziltepe and R. Sasisekharan, *Nature*, 2005, 436, 568-572.
25. A. K. Gupta and M. Gupta, *Biomaterials*, 2005, 26, 3995-4021.
26. M.-H. Hsiao, T.-H. Tung, C.-S. Hsiao and D.-M. Liu, *Carbohydrate Polymers*, 2012, 89, 632-639.
27. S.-H. Hu, B.-J. Liao, C.-S. Chiang, P.-J. Chen, I. W. Chen and S.-Y. Chen, *Advanced Materials*, 2012, 24, 3627-3632.
28. E. Lee, H. Kim, I. H. Lee and S. Jon, *Journal of Controlled Release*, 2009, 140, 79-85.
29. T.-Y. Liu, S.-Y. Chen, Y.-L. Lin and D.-M. Liu, *Langmuir*, 2006, 22, 9740-9745.
30. K.-H. Liu, S.-Y. Chen, D.-M. Liu and T.-Y. Liu, *Macromolecules*, 2008, 41, 6511-6516.
31. Y.-J. Wang, Y.-C. Chien, C.-H. Wu and D.-M. Liu, *Molecular Pharmaceutics*, 2011, 8, 2339-2349.
32. Y.-J. Wang, H.-Y. Lin, C.-H. Wu and D.-M. Liu, *Molecular Pharmaceutics*, 2012, 9, 2268-2279.
33. N. A. Peppas, *Pharmaceutica acta Helvetiae*, 1985, 60, 110-111.
34. P. Costa and J. M. Sousa Lobo, *European Journal of Pharmaceutical Sciences*, 2001, 13, 123-133.
35. J. Griffiths, *British journal of cancer*, 1991, 64, 425.
36. M. Schindler, S. Grabski, E. Hoff and S. M. Simon, *Biochemistry*, 1996, 35, 2811-2817.
37. O. Seksek and J. Bolard, *Journal of Cell Science*, 1996, 109, 257-262.
38. M. Aguedo, Y. Waché and J.-M. Belin, *FEMS Microbiology Letters*, 2001, 200, 185-189.

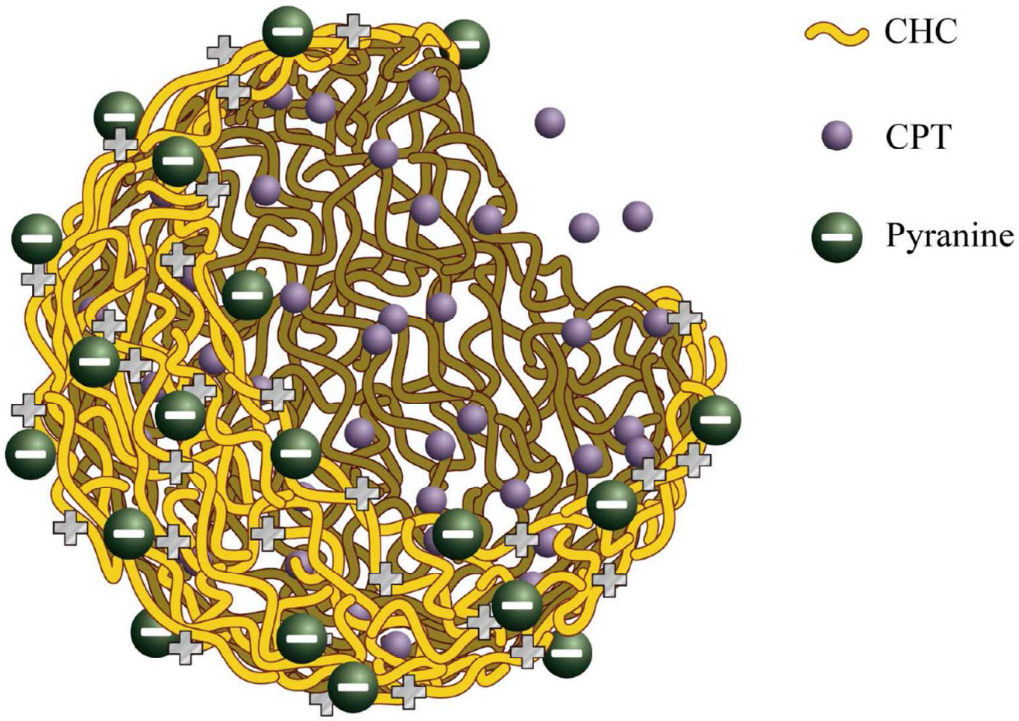

Scheme 1. The structure of CHC-PY nanoparticle.

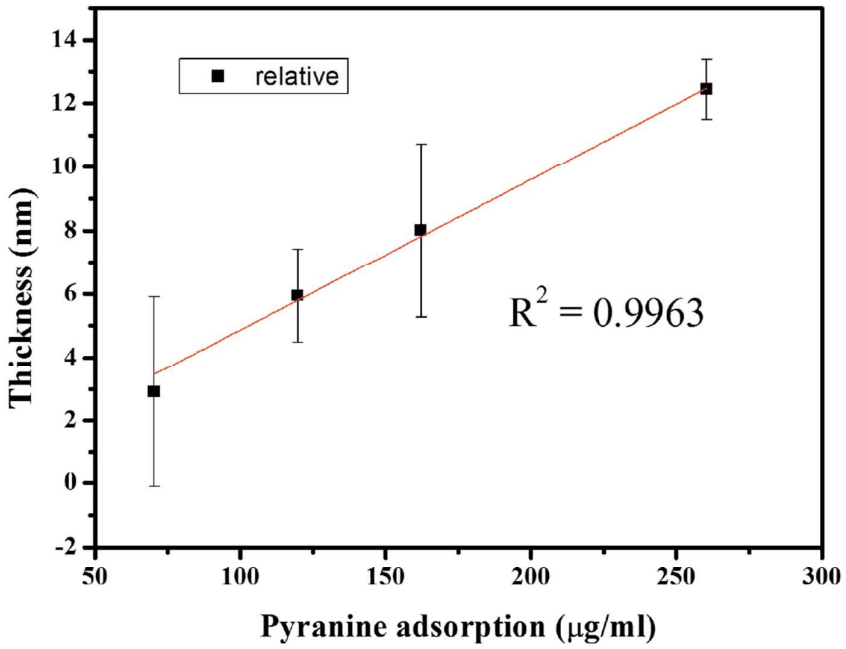

Fig 1. The pyranine shell thickness increases linearly with increasing amount of pyranine deposition on the CHC core.

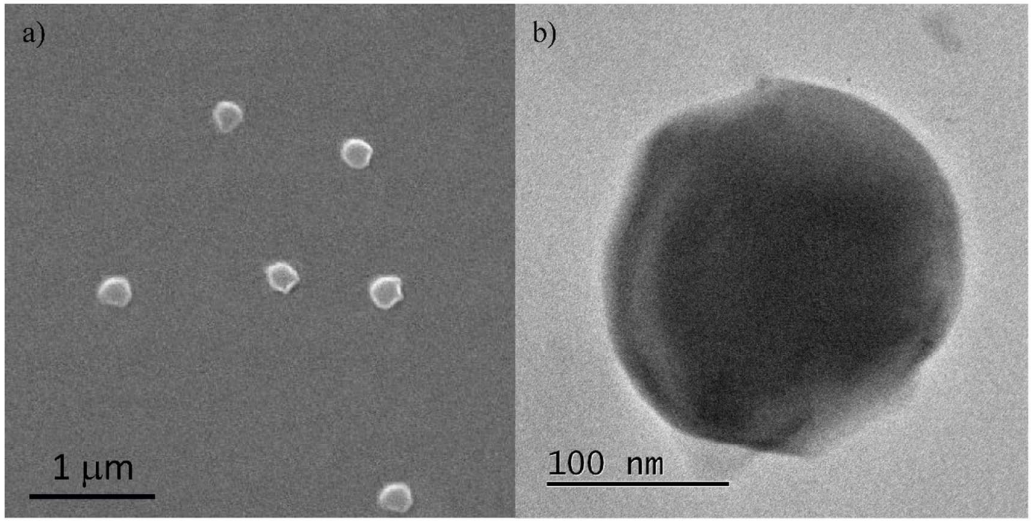

Fig 2. Morphology of CHC-PY nanoparticles with (a) SEM image of self-assembled CHC nanoparticle and b) TEM image of CHC-PY0.2 nanoparticles, showing a pyranine shell after rapid electrostatic deposition.

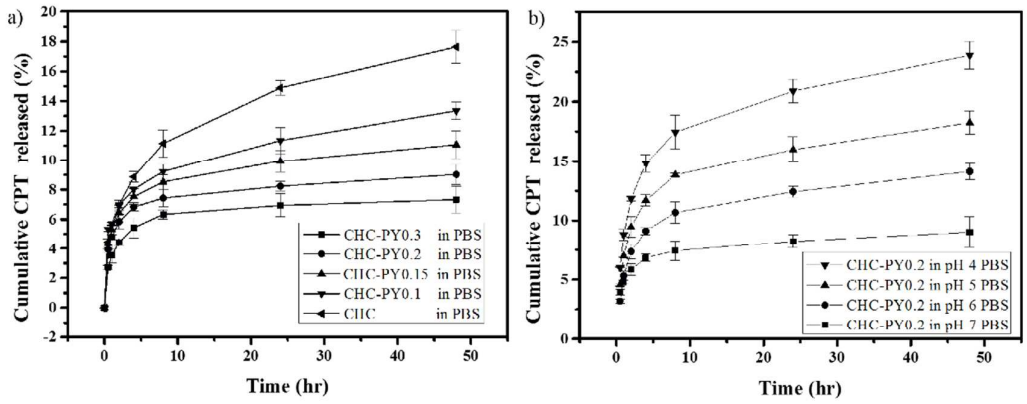

Fig 3. a) The release profile of CPT (0.1mg/mL) from various pyranine concentrations (0.1, 0.15, 0.2, 0.3 mg/mL) in PBS solution. b) The release profile of CHC-PY0.2 with CPT (0.1mg/mL) from PBS buffer with different pH values (4, 5, 6, and 7).

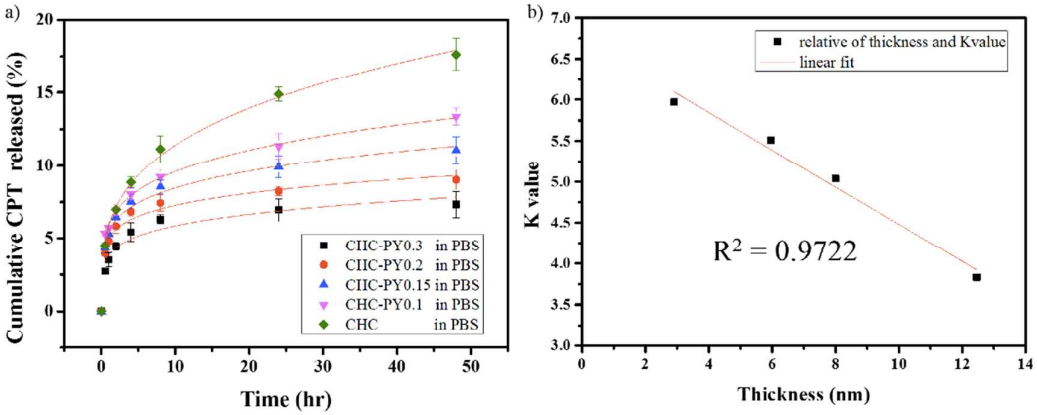

Fig 4. a) The release kinetics for various pyranine concentrations. b) The rate constant declines linearly with increasing pyranine shell thickness.

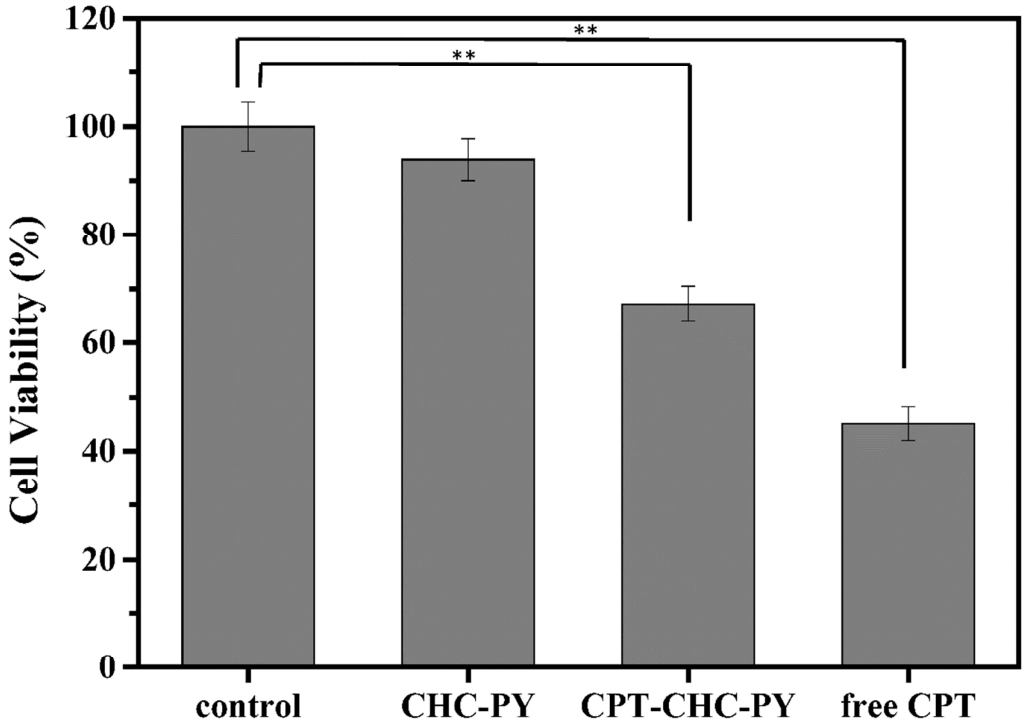

Fig 5. Cell viability of A549 cells incubated with 2 mg/ml CHC-PY0.2 nanoparticles, 2 mg/ml CPT-CHC-PY0.2 nanoparticles (the total quantity of CPT in the nanoparticle is), and 192.2 μg/ml free CPT for 24 hours (n = 3).

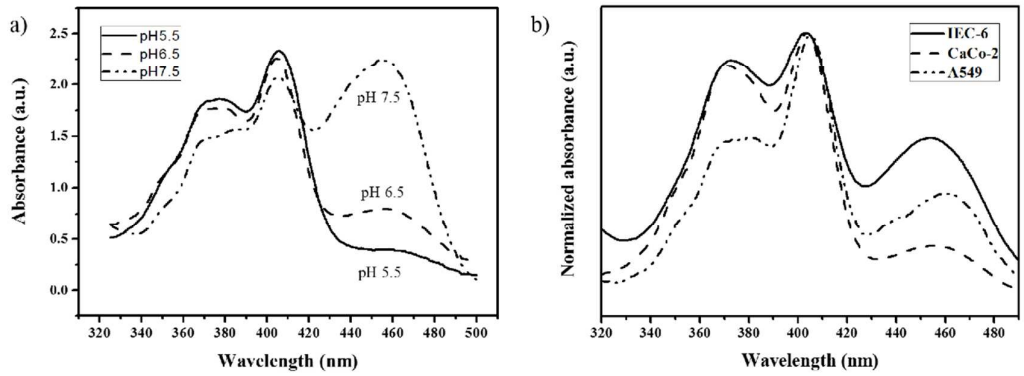

Fig 6. Intracellular pH measurement with CHC-PY0.2 nanoparticles. Here a) normalized excitation fluorescence spectra of CHC-PY0.2 in buffer of pH 5.5, pH 6.5 and pH 7.5, b) fluorescence intensity of CHC-PY nanoparticles in different cell lines.

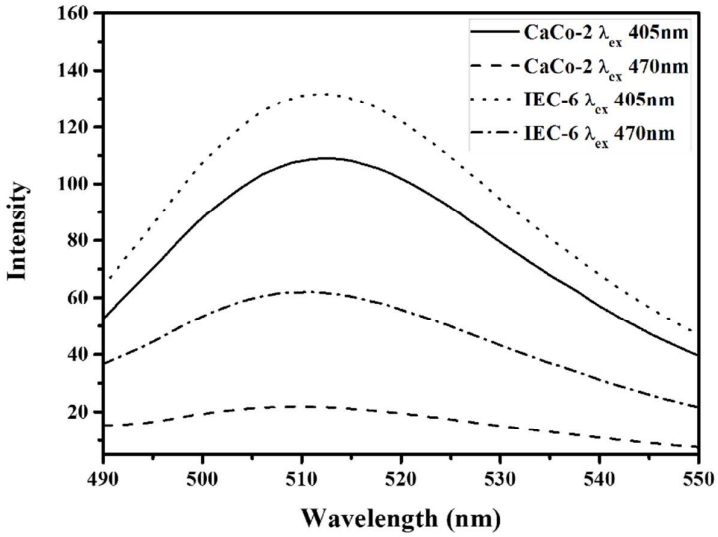

Fig 7. The emission intensity of CHC-PY0.2 in IEC-6 cells or CaCo-2 cells by fluorescence spectrophotometer. After normalize with λ_{ex} 405nm, the intensity of IEC-6 λ_{ex} 470nm was higher than CaCo-2 λ_{ex} 470nm about 2.5 times.

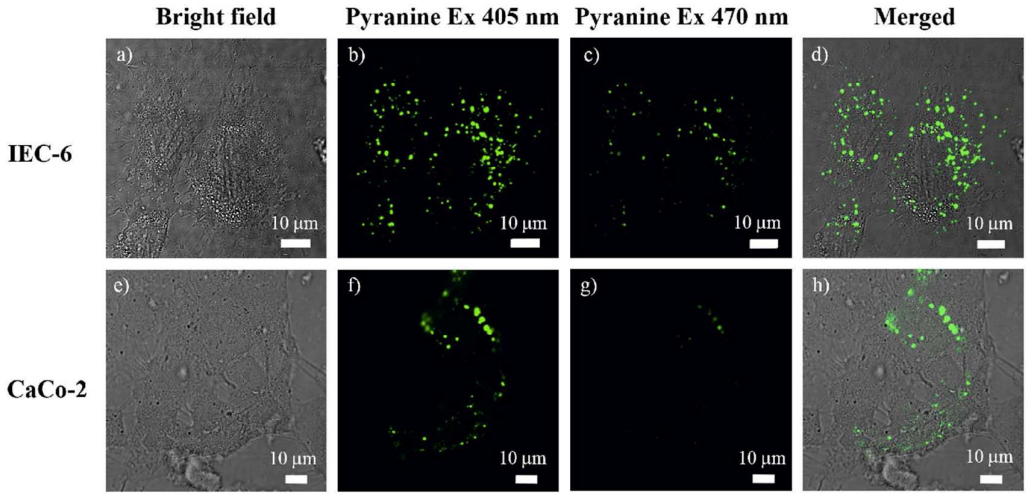

Fig 8. Confocal microscope image of CHC-PY0.2 in IEC-6 cells (a, b, c) or CaCo-2 cells (e, f, g). a), e) bright field image of two kinds of cells; b), f) the CHC-PY fluorescence images using 405 nm excitation; c), g) using 470 nm excitation.

Table of contents entry

A pH-responsive Amphiphilic Chitosan-Pyranine Core-Shell Nanoparticle for Control Drug Delivery, Imaging and Intracellular pH Measurement

Hao-Syun Chou[1], Meng-Hsuan Hsiao[1], Wei-Yang Hung[1], Tin-Yo Yen[2], Hui-Yi Lin[3*], Dean-Mo Liu[1*]

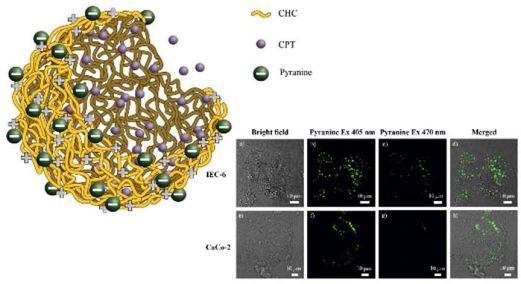

This new type of CHC-PY core-shell nanoparticle provides multiple functionality where a synergistic performance of nanotherapeutics, imaging and even diagnosis at a cellular resolution can be achieved simultaneously.